# 14.2 RETRIEVAL OF CLOUD GEOMETRICAL PROPERTIES USING ADEOS-II/GLI


Makoto Kuji*[a] and Teruyuki Nakajima[b]

[a] Dept. of Information and Computer Sciences, Nara Women's Univ., Japan

[b] Center for Climate System Research, Univ. of Tokyo, Japan



## ABSTRACT

Clouds play a crucial role in the climate system. The investigation of their radiative properties on the cloud optical, microphysical, and geometrical characteristics is of great interest. Here, top height, base height, and geometrical thickness of cloud layer are considered as cloud geometrical properties.

Several studies show that information of some spectral regions including oxygen A-band, enables us to retrieve the cloud geometrical properties as well as the optical thickness and the effective particle radius of cloud. In this study, an algorithm is presented to retrieve simultaneously the cloud optical thickness, effective particle radius, top height, and geometrical thickness of cloud layer with the spectral information of visible, near infrared, thermal infrared, and oxygen A-band channels.

This algorithm was applied to ADEOS-II / GLI dataset so as to retrieve global distribution of cloud geometrical properties. The retrieved results around Japan are validated with in situ observations. The retrieved and in-situ observed values are comparable in order of magnitude, but it is necessary to investigate the results in detail to improve the algorithm. This study will expand to the global analysis and is anticipated to contribute to the earth climate studies in terms of cloud optical, microphysical, and geometrical properties.


## 1. INTRODUCTION

Global observations with satellites have revealed the radiation budget at top of the atmosphere of the earth. But different studies on the estimation of surface radiation budget have in general failed to yield results consistent between themselves. It is believed that the uncertainty in the determination cloud base height is one of the sources of this inconsistence, as well as water vapour anomalous absorption and aerosol properties.

To determine cloud top height, many investigations are carried out with the utilization of oxygen absorption spectral band and other spectral bands. Investigation using oxygen absorption spectral bands has a chronologically long history. Yamamoto and Wark (1961) suggested the utilization of oxygen A-band information to estimate the cloud top height rather than the carbon dioxide due to the mixing of its absorption lines with the ones of water vapour. Saiedy *et al.* (1967) studied the cloud top determination with hand-held spectrograph-camera observation by Gemini-5 astronauts and suggested the correction method for the photon penetration with the solar zenith, viewing and azimuthal angles. Curran *et al.* (1981) showed that the multichannel scanning radiometer with two channels in oxygen A-band, had the capability of cloud top altitude detection. Wu (1985) investigated the cloud top height retrieval using the spectral observation around the oxygen A-band. His approach was called the radiance ratio method and he discussed the correction of photon penetration effect that had to be taken into consideration for the method. Fischer and Grassl (1991) and Fischer *et al.* (1991) made a more detailed analysis for cloud top estimation using the oxygen A-band validated with simultaneous LIDAR observation. On the other hand, Hayasaka *et al.* (1995) developed a retrieval algorithm of cloud geometrical thickness from a measured liquid water path and equivalent width of 0.94 µm water vapor absorption band. The algorithm was applied to aircraft observations to retrieve the geometrical thickness, and the results were smaller than


* *Corresponding author address:* Makoto Kuji, Nara Women's Univ., Dept. of Information and Computer Sciences, Nara, Japan, 630-8506; e-mail: makato@ics.nara-wu.ac.jp

those observed by eye. Asano *et al.* (1995) showed a retrieval algorithm of cloud optical, microphysical, and geometrical parameters simultaneously using aircraft flux observations. For the preparation of the launch of Advanced Earth Observing Satellite-II (ADEOS-II) Global Imager (GLI), Nakajima *et al.* (1998) showed the sensitivity estimation of the oxygen A-band radiance to be observed from space to the geometrical parameters. Recently, Kuji *et al.* (2002) developed an algorithm to retrieve the cloud optical thickness, effective particle radius, top height, and geometrical thickness of cloud layer simultaneously using information of four spectral regions such as the visible, near infrared, oxygen A-band and thermal infrared, and it was applied to the airborne observation. The retrieved results were validated with LIDAR observation and they were comparable to each other. In the present study, the algorithm was applied to the GLI data and the preliminary results are discussed.

## 2. SATELLITE DATA

The GLI observation and its spectral specification concerning our analyses are described in this section.

GLI has 36 channels from visible to thermal infrared spectral region. Relevant spectral specification of GLI is concisely shown in Table 1. In the analysis, the following four channels are mainly used: visible (Ch.13), oxygen A-band (Ch.17; P-branch), near infrared (Ch.29), and thermal infrared (Ch.35). A middle infrared channel (Ch. 30) is an alternative for near infrared channel (Ch. 29), which is also sensitive to the cloud particle size. A strong water vapour absorption channel (Ch. 27) in the near infrared spectral region is utilized to screen out upper-level clouds (Gao *et al.* 2000).

**Table 1.** Spectral specifications of GLI. Relevant Channels for this study.

| Channel number | Wavelength ($\mu$m) | Spectral features | Instantaneous field of view (km) |
|---|---|---|---|
| 13 | 0.679 | Visible | 1 |
| 17 | 0.762 | Oxygen A-band | 1 |
| 27 | 1.38 | Water Vapor Absorption | 1 |
| 29 | 2.19 | Near Infrared | 0.25 |
| 30 | 3.72 | Middle Infrared | 1 |
| 35 | 10.8 | Thermal Infrared | 1 |

A marine cloud system extended over the west Pacific Ocean on March 20, 2003. Targeting this cloud system, early stage observation was conducted with ADEOS-II / GLI. Figure 1 illustrates an imagery of the scene. The scene ID is A2GL10303200612OD1 and observation was in descending mode. The image center is located around 27˚N and 135˚E. The latitude range is 18.5 to 35.5 ˚N and the longitude from 125.1 to 145.9 ˚E for the scene. The time when observation was carried out was around 1041 Japan Standard Time (JST). That corresponds to 0141 in Universal Time Coordinated (UTC; JST=UTC+0900). There are around two hundred thousand pixels; 1236 pixels in cross-track direction and 1656 in along-track direction. In Fig. 1, the western part of Japan islands in left-top portion and a large cloudy region in the central portion can be seen. By Japan Aerospace Exploration Agency (JAXA), a routine analysis was already carried out for the scene, which indicated that the cloud optical thickness were several tens; cloud droplet radii were about several micrometers, and cloud top temperatures were around 260-270K.

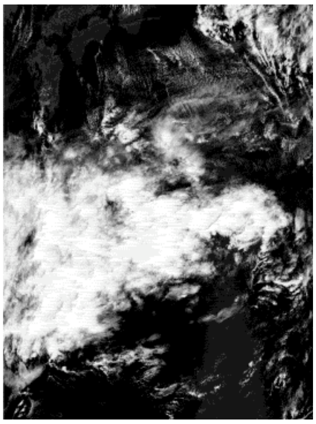

**Figure 1.** An imagery of ADEOS-II / GLI. March 20, 2003 around south of Japan.

## 3. METHODOLOGY

The retrieval algorithm and analysis flow are described in this section.

### 3.1 *The retrieval algorithm*

Retrieval algorithm and its flow are based upon the one that was developed for the airborne data (Kuji *et al.* 2002). The algorithm principally utilizes four channels such as visible, oxygen A-band, near infrared, and thermal infrared available in GLI properly. The algorithm is applied to the GLI data in this study. Figure 2 illustrates imageries of those four channels.

The analyzed data are actually resampled every 12 pixels in both along- and cross-track direction out of original data since scan geometry (solar and sensor zenith angles, and azimuthal angles) and location information (latitude, longitude, and observation time) are provided in that interval

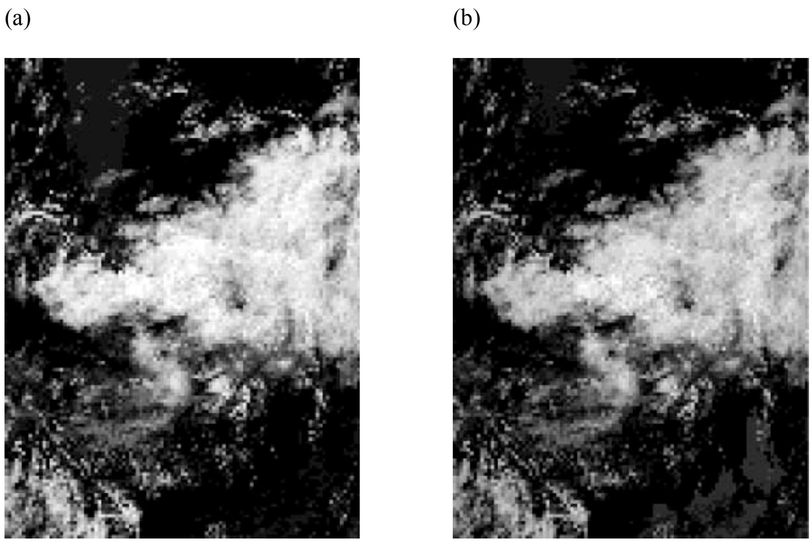

**Figure 2.** Imageries of analyzed data: (a) Ch. 13 (0.679 μm) and (b) Ch. 17 (0.762 μm).

(c) (d)

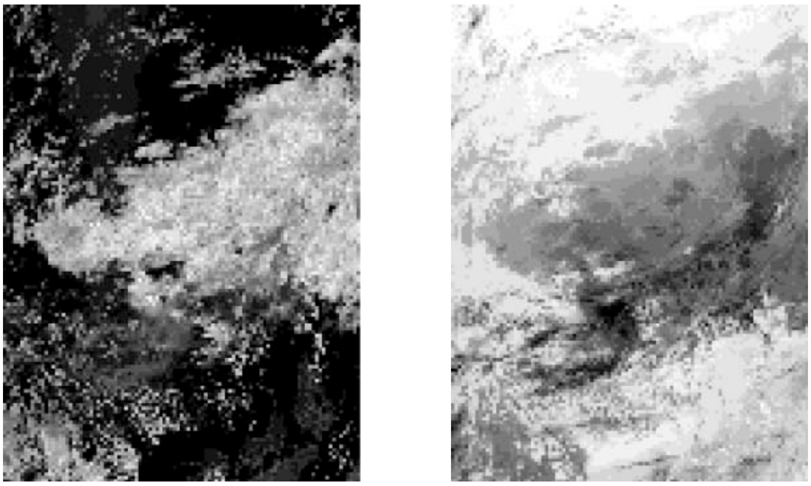

**Figure 2.** (Continued) Imageries of analyzed data: (c) Ch. 29 (2.19 μm) and (d) Ch. 35 (10.8 μm).

### 3.2 *Upper-level cloud screening*

The retrieval algorithm assumes a single layer model with water cloud. The upper-level ice cloud over lower-level water cloud may cause retrieval error for geometrical parameters in particular (Kuji *et al.* 2002). To screen out the upper-level ice cloud, the 1.38-μm water vapor absorption channel information is useful (Gao *et al.* 2000). Figure 3 shows the imagery of that channel which is supposed to reveal the upper-level cloud layer. In such a strong water vapour absorption band, reflected radiance from surface, lower-level cloud, or aerosol, is absorbed almost completely since water vapor exists in the lower level atmosphere. As a result, only upper-level cloud or aerosol, that is, scattering particles, is seen brightly in Fig. 3. The upper-level cloud existence is also suggested in Fig. 2 (d). In the thermal infrared spectral region, radiances for upper-level cloud are seen as darker since temperature usually decreases gradually as altitude increases. It can be seen the brighter portion of Fig.3 corresponds to the darker portion in Fig. 2 (d).

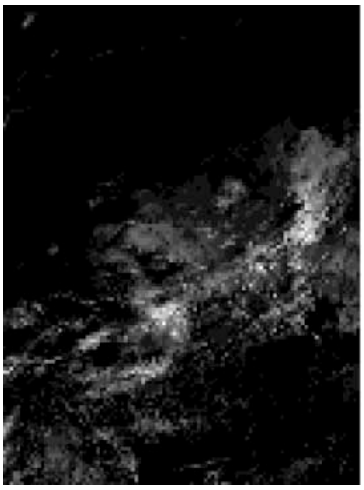

**Figure 3.** Imageries of analyzed data: Ch. 27 (1.38 μm).

At this preliminary analysis, tentative upper-level cloud screening was carried out, that is, analyzed pixels were selected satisfying the condition that Ch. 27 radiance is less than 5.05 (W $m^{-2}$ $sr^{-1}$ $\mu m^{-1}$), whose value is one standard deviation in the scene.

### 3.3 *Alternative channel*

In the retrieval algorithm, near infrared Ch. 29 (2.19 μm) is utilized to retrieve cloud particle size principally. But the instantaneous field of view (IFOV) of the channel is 0.25 km, while it is 1 km for other three channels. There is an alternative middle infrared channel, Ch. 30 (3.72 μm) with 1-km IFOV. The retrieval algorithm is capable of employing of both middle and near infrared channels. Figure 4 shows an imagery of alternative channel, Ch. 30 (3.72 μm).

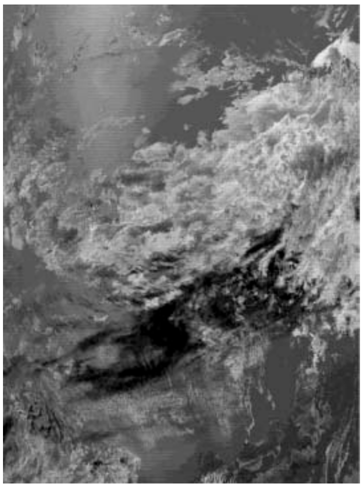

**Figure 4.** Imageries of analyzed data: Ch. 30 (3.72 μm).

## 4. RESULTS

With the retrieval algorithm with four spectral channels (visible, oxygen A-band, near infrared, and thermal infrared), following four geophysical parameters of cloud layer such as cloud optical thickness, effective particle radius, cloud top height, and cloud geometrical thickness are directly retrieved. Liquid water path and bottom height of cloud layer are derived from the above properties as by-products.

Figure 5 illustrates the retrieved results of (a) optical thickness of cloud, (b) effective particle radius, and (c) liquid water path, respectively. The liquid water path is derived from the optical thickness of cloud and effective particle radius using Eq. (1).

Cloud optical thickness $\tau_c$ and effective droplet radius $r_e$ (μm) are essentially retrieved using visible and near infrared spectral radiance information, and also liquid water path (LWP in g m$^{-2}$) as a by-product from the relationship:[12]

$$LWP = \frac{2}{3}\tau_c \cdot r_e \cdot \rho_w, \qquad (1)$$

where $\rho_w$ (g m$^{-3}$) is the density of water.

Figure 5 also illustrates (d) top height $Z_t$ (km), (e) the geometrical thickness $D$ (km) of a cloud layer. In this figure, (f) cloud bottom height $Z_b$ (km) is derived from the cloud top height and the cloud geometrical thickness as follows:

$$Z_b = Z_t - D. \qquad (2)$$

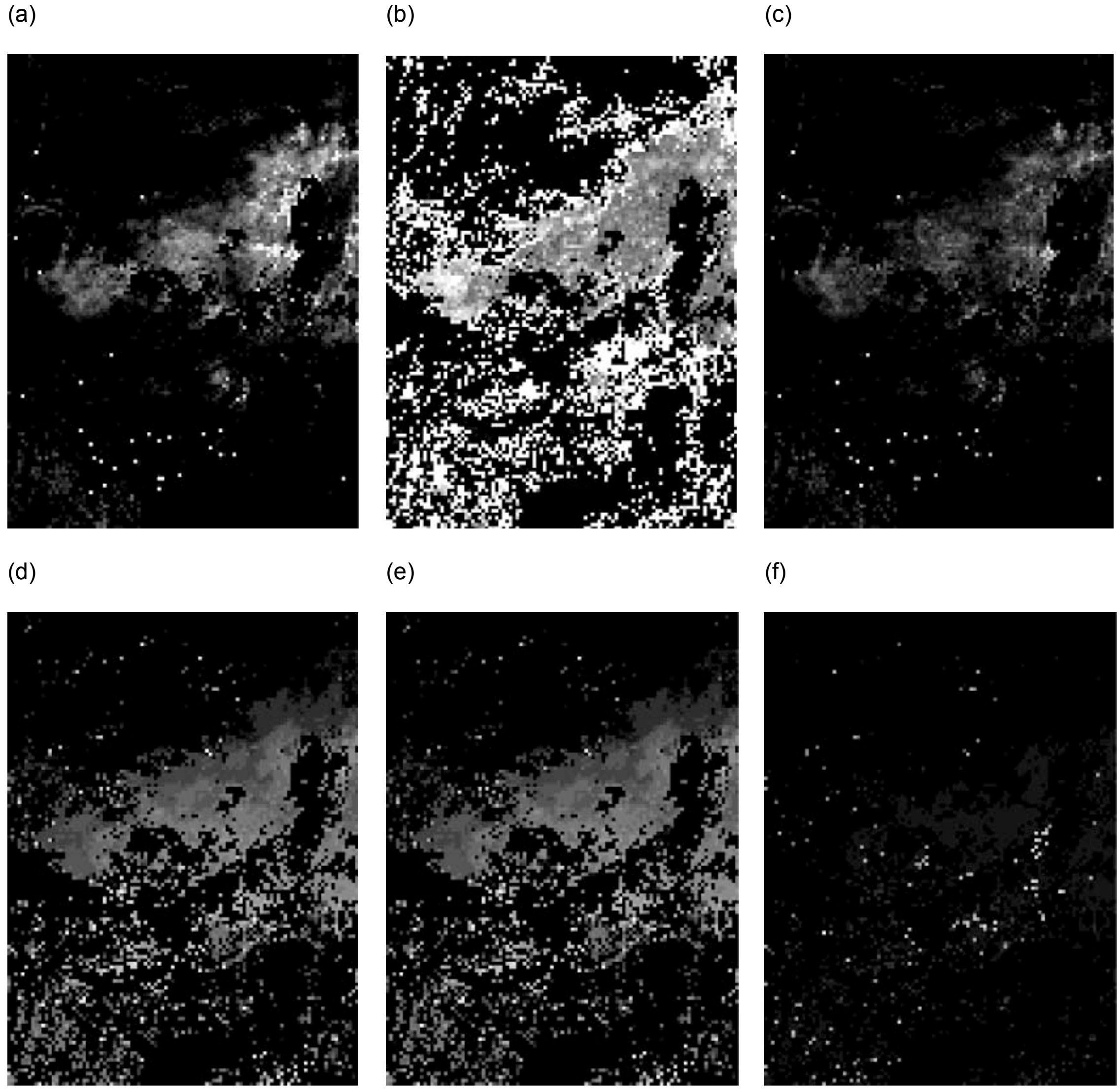


**Figure 5.** Retrieved results: (a) optical thickness of cloud, (b) effective particle radius, (c) liquid water path, (d) cloud top height, (e) cloud geometrical thickness, and (f) cloud bottom height. Liquid water path and cloud bottom height are by-products.

The results in Fig. 5 were retrieved after upper-level cloud screening. For cloud particle size, retrieval range is limited from 1 to 16 μm since cloud particle size are retrieved unrealistically large otherwise, for broken cloud fields in particular. Table 2 summarizes the retrieval results.

**Table 2.** Retrieved results.

| Properties | Average | Standard Deviation |
|---|---|---|
| $\tau_c$ (678nm) | 22.6 | 25.9 |
| $r_e$ ($\mu$m)** | 12.1 | 4.5 |
| LWP (g $m^{-2}$)* | 145 | 158 |
| $Z_t$ (km) | 3.4 | 1.5 |
| D (km) | 3.0 | 1.4 |
| $Z_b$ (km)* | 0.43 | 0.52 |

* Liquid water path and cloud bottom heights are by-products.

** Effective particle radius is retrieved within 1-16μm range in the procedure.

## 5. DISCUSSION

The retrieved results are discussed in this section.

### 5.1. *Comparison of the retrieved results with near and middle infrared channels*

Simultaneous retrieval of optical thickness of cloud and effective particle radius from the visible and near (or middle) infrared spectral information has been already investigated in previous studies (Nakajima and King 1990; Nakajima *et al.* 1991; Nakajima and Nakajima 1995; Kuji *et al.* 2000). ADEOS-II / GLI has both near infrared (2.19μm) and middle infrared (3.72μm) channels, which have different IFOV with 0.25 and 1 km, respectively. In addition, there is also the difference of spectral features that the middle infrared channel contains a thermal (or terrestrial) radiation component that is not considered for the near infrared channel. The comparison with alternative usage of these two channels serves to check robustness or self-consistency of the algorithm.

Figure 6 illustrates the retrieved results of only cloud particle size using four spectral channels including middle infrared (3.72μm) instead of the near infrared (2.19μm) channel.

**Figure 6.** Retrieved effective particle size with Ch. 30 (3.72 μm) instead of Ch. 29 (2.19 μm).

Comparing Fig. 6 to Fig. 5 (b), it can be seen that the fine structure in Fig. 5 (b) has been lost in Fig. 6. The middle infrared information retrieves larger values than the near infrared since cloud particle sizes larger than 16μm is forced to be 16μm in the retrieval procedure. There is another explanation for the difference, namely that the 1-km IFOV of the middle infrared channel equalizes the radiances while the finer IFOV (0.25 km) of the near infrared channel could detect finer radiance or cloud particle variations. It is necessary to validate the retrieved results and refine the procedure to retrieve cloud particle size in future. The statistics of retrieved results are summarized in Table 3.

**Table 3.** Comparison of retrieved products between near infrared and middle infrared channels.

| Channels | Ch. 29 (2.19 μm) | | Ch. 30 (3.72 μm) | |
|---|---|---|---|---|
| Properties | Average | Standard Deviation | Average | Standard Deviation |
| $\tau_c$ (0.678 μm) | 22.6 | 25.9 | 25.7 | 25.8 |
| $r_e$ (μm)** | 12.1 | 4.5 | 13.2 | 5.6 |
| LWP (g $m^{-2}$)* | 145 | 158 | 267 | 282 |
| $Z_t$ (km) | 3.4 | 1.5 | 3.4 | 1.5 |
| D (km) | 3.0 | 1.4 | 2.9 | 1.3 |
| $Z_b$ (km)* | 0.43 | 0.52 | 0.51 | 0.70 |

* Liquid water path and cloud bottom heights are by-products.

** Effective particle radius is retrieved within 1-16μm range in the procedure.

One of the remarkable features seen in Table 3 is that cloud geometrical properties using channel 29 or channel 30 are identical to each other. Liquid water path, on the other hand, has a great difference in a factor about two. Since liquid water path is a by-product estimated with Eq. (1), the difference is attributed to retrieval uncertainty of optical thickness and cloud particle size. In principle, darker radiance in near (middle) infrared channel is interpreted as larger particle size. The retrieval error is anticipated to be more severe for the middle infrared channel with larger IFOV, under broken cloud field in particular.

### 5.2 *Comparison of the retrieved results with in-situ observations*

A field campaign, so-called APEX-E3, was conducted from March to April, 2003 based at Amami Oshima. Here, preliminary comparison between GLI derived and in-situ, e.g., ground-based and aircraft, observations is described. Aircraft observation was carried out around Amami Oshima island (28.4˚N, 129.68˚E, and 50m a.s.l.). The airborne observation yielded effective particle radius was around 5μm. The GLI retrieval indicates the particle size around Amami Ooshima was around 12 to 15 μm in Table 3. Since the GLI result is a statistics on a scene basis, a match-up comparison is necessary as one of the future tasks.

At Amami Oshima, on the other hand, several kinds of ground-based measurement were also carried out, such as radiation measurements for surface radiation budget, and vertical profiling of the atmosphere using active sensors. The instrumentation included a pyranometer and a microwave radiometer, as well as a lidar and a radar. Figure 7 shows an example of lidar and radar observations.

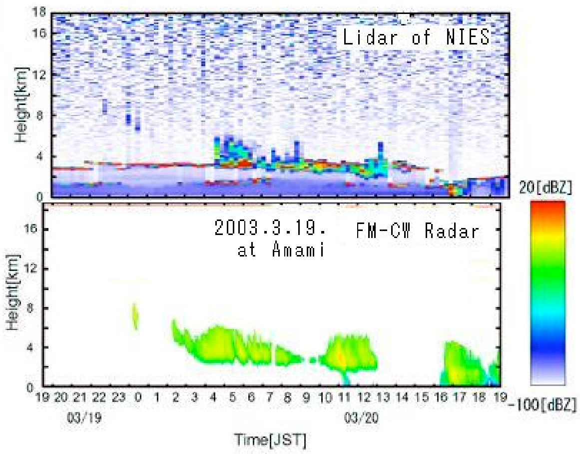


**Figure 7.** An example of round-based observations. Top panel: LIDAR observation conducted by NIES in Japan; Bottom panel: FM-CW Radar observation by Chiba University in Japan. These observations were carried out under APEX-E3 campaign. FM-CW means Frequency Modulated – Continuous Wavelength. These results were provided by courtesy of Dr. Sugimoto of NIES and Prof. Takano of Chiba University. The top and bottom panels show a lidar signal in arbitrary unit and a radar echo, respectively.

During the observation, ADEOS-II flew over the Amami island around 10:30 AM at Japanese Standard Time. Comparing the retrieved cloud top (3.4km) and bottom (0.43km with 2.19μm; 0.51km with 3.72μm) height to the in-situ lidar and radar observation, GLI underestimated cloud top and bottom heights. A more detailed comparison, using results corresponding to Amami Ooshima island site pixels, is needed.

## 6. CONCLUDING REMARKS

The ADEOS-II / GLI data were preliminary analyzed to retrieve the cloud geometrical properties as well as optical and microphysical ones. In this preliminary analysis stage, the retrieved results seem to be reasonable as a whole, but it is suggested that algorithm improvement is necessary to retrieve cloud particle sizes with higher accuracy. The geometrical properties are, on the other hand, self-consistent even with an alternative channel selection. The retrieved results around Japan are validated with in situ observations. The retrieved and in-situ observed values are comparable in order of magnitude, but it is necessary to investigate the results in detail to improve the algorithm. This study will expand to the global analysis and is anticipated to contribute to the earth climate studies in terms of cloud optical, microphysical, and geometrical properties.

*ACKNOWLEDGEMENTS* This study is funded by Japan Aerospace Exploration Agency (JAXA). Authors thank Mr. Hiroshi Yatagai of JAXA for the GLI data processing. Authors also thank Dr. T. Y. Nakajima of JAXA / Earth Observation Research/Application Center (EORC) for advice on calculations of look-up tables. The results of LIDAR and RADAR are provided by Dr. N. Sugimoto of National Institute of Environmental Study (NIES), Japan, and Prof. T. Takano of Chiba Univ., Japan, respectively.

## REFERENCES

Asano, S., M. Shiobara, and A. Uchiyama, 1995: Estimation of Cloud Physical Parameters from Airborne Solar Spectral Reflectance Measurements for Stratocumulus Clouds, *J. Atmos. Sci.,* **52,** 3556-3576.

Curran, R. J., H. L. Kyle, L. R. Blaine, J. Smith, and T. D. Clem, 1981: Multichannel scanning radiometer for remote sensing cloud physical parameters, *Rev. Sci. Instrm.,* **52,** 1546-1555.

Fischer, J., and H. Grassl, 1991: Detection of Cloud-Top Height from Backscattered Radiances within the Oxygen A Band. Part 1: Theoretical Study, *J. Appl. Meteor.,* **30,** 1245-1259.

Fischer, J., W. Cordes, A. Schimits-Peiffer, W. Renger, and P. Moerl, 1991: Detection of Cloud-Top Height from Backscattered Radiances within the Oxygen A Band. Part 2: Measurements, *J. Appl. Meteor.,* **30,** 1260-1267.

Gao, G. -C., A. F. H. Goetz, and W. J. Wiscombe, 2000: Cirrus cloud detection from airborne imaging spectrometer data using 1.38 μm water vapor band, *Geophys. Res. Lett.*, **20**, 301-304.

Hayasaka, T., T. Nakajima, Y. Fujiyoshi, Y. Ishizaka, T. Takeda, and M. Tanaka, 1995: Geometrical Thickness, Liquid Water Content, and Radiative Properties of Stratocumulus Clouds over the Western North Pacific, *J. Appl. Meteor.,* **34,** 460-470.

Kuji, M., T. Hayasaka, N. Kikuchi, T. Nakajima, and M. Tanaka, 2000: The retrieval of effective particle radius and liquid water path of low-level marine clouds from NOAA AVHRR data, *J. Appl. Meteor.,* **39,** 999-1016.

Kuji, M., T. Nakajima and S. Mukai, 2002: Retrieval of cloud geometrical properties using optical remote sensing data, *Proc. SPIE*, **4882,** 194-204.

Nakajima, T., and M. D. King, 1990: Determination of the optical thickness and effective particle radius of clouds from reflected solar radiation measurements. Part I: Theory, *J. Atmos. Sci.,* **47,** 1878-1893.

Nakajima, T., M. D. King, J. D. Spinhirne, and L. F. Radke, 1991: Determination of the optical thickness and effective particle radius of clouds from reflected solar radiation measurements. Part II: Marine Stratocumulus Observations, *J. Atmos. Sci.,* **48,** 728-750.

Nakajima, T. Y., and T. Nakajima, 1995: Wide-area determination of cloud microphysical properties from NOAA AVHRR measurements for FIRE and ASTEX regions, *J. Atmos. Sci.,* **52,** 4043-4059.

Nakajima, T. Y., T. Nakajima, M. Nakajima, H. Fukushima, M. Kuji, A. Uchiyama, and M. Kishino, 1998: The optimization of the Advanced Earth Observing Satellite II Global Imager channels by use of radiative transfer calculations, *Appl. Opt.,* **37,** 3149-3163.

Saiedy, F., H. Jacobowitz, and D. Q. Wark, 1967: On Cloud-Top Determination from Gemini-5, *J. Atmos. Sci.,* **35,** 63-69.

Wu, M. -L. C., 1985: Remote Sensing of Cloud-Top Pressure Using Reflected Solar Radiation in the Oxygen A-Band, *J. Climate Appl. Meteor.,* **24,** 539-546.

Yamamoto, G., and D. Q. Wark, 1961: Discussion of the Letter by R. A. Hanel, 'Determination of Cloud Altitude from a Satellite', *J. Geophys. Res.,* **66,** 3596.